CrossMark

INVITED PAPER

Se-doped $Ge_{10}Sb_{90}$ for highly reliable phase-change memory with low operation power

Jeong Hoon Kim, Dae-Seop Byeon, and Dae-Hong Ko[a)]
Department of Materials Science and Engineering, Yonsei University, Seoul 120-749, Republic of Korea

Jeong Hee Park
Process Development Team, Semiconductor R&D Division, Samsung Electronics Co., Ltd., Hwasung-City, Kyungki-Do 445-701, Korea

(Received 17 February 2017; accepted 11 May 2017)

In this study, we propose a Se-incorporated $Ge_{10}Sb_{90}$ as a phase-change material for phase-change memory (PCM) with high reliability and low operation power. We investigated the effect of the Se concentration on the thermal and electrical properties of Se-doped $Ge_{10}Sb_{90}$ films by varying the Se concentration from 0 to 20 at.%. The crystallization temperature, crystallization activation energy, and maximum ten-year data retention temperature increased with the increasing Se, thus demonstrating the improved thermal stability of Se-doped $Ge_{10}Sb_{90}$ films with higher Se contents. More Se also increased the rate factor, band gap, threshold voltage, and load resistance. In addition, the crystallization speed, programming window, and resistances of both the amorphous and crystalline states increased with the increasing Se concentration. In contrast, the reset current decreased with the increasing Se concentration. These results demonstrate that Se-doped $Ge_{10}Sb_{90}$ is a highly promising material for PCM applications.

I. INTRODUCTION

As the portable electronic device, artificial intelligence, and IoT (Internet of Things) markets rapidly expand, so does the demand for nonvolatile memory. Flash memory technology, which is currently being used the most for nonvolatile memory applications, has faced physical limitations and downscaling issues. Therefore, many alternative nonvolatile memory technologies have been investigated such as phase-change RAM (PRAM), ferroelectric RAM (FeRAM), and resistance RAM (RRAM).[1] Among next-generation nonvolatile memories, PRAM has been considered the most promising candidate due to its high scalability, cost-effectiveness, good compatibility with CMOS technologies, good endurance, and nonvolatility.[2–8] The principle of PRAM operation relies on the difference between the electrical resistances of the amorphous and crystalline states, which represent the logic states '1' and '0', respectively.[9] Currently, PRAM uses an electrical pulse to melt the phase-change material by joule heating for a RESET operation. Therefore, high power consumption is a major obstacle to developing high-density PRAM.[10] However, $Ge_2Sb_2Te_5$, which is the most common phase-change material used in PRAM, requires a high reset current. Because this material has a high melting temperature and low crystalline resistivity,[11,12] various strategies have been investigated to reduce the reset current, such as structural and material modifications. In the literature, Sb-rich alloys are considered to exhibit growth-dominated crystallization behavior, which could guarantee fast operation speed. Therefore, Sb-rich GeSb phase-change materials have been investigated, but their high reset current and low thermal stability are obstacles that must be overcome to be used in PRAM. In this paper, we chose Se and $Ge_{10}Sb_{90}$ as the dopant and phase-change material, respectively, because $Ge_{10}Sb_{90}$ exhibits a fast phase transformation. The Te-doped GeSb alloys have been extensively studied and reported previously.[13–15] Even though Se is just above Te in the same column of the periodic table (i.e., chalcogenides), the melting temperature of Se (T_m = 221 °C) is lower than that of Te (T_m = 449 °C), and the Ge–Se bond enthalpy (235 kJ/mol) is higher than that of Ge–Te (157 kJ/mol). Since a lower melting temperature enables the use of a lower reset current, and a higher bond enthalpy can improve the thermal stability, we expect that Se doping would be more advantageous for the low-power and high-reliability memory devices than the Te doping reported in previous studies. Furthermore, according to previous reports, both the resistance and crystallization temperature of this system increase with increased Se concentration.[16,17] Therefore, PRAM devices constructed with Se-doped $Ge_{10}Sb_{90}$ films are expected to consume less power and be more thermally stable than device constructed from conventional $Ge_2Sb_2Te_5$. The concentration of Se in our

Contributing Editor: Don W. Shaw
[a)]Address all correspondence to this author.
e-mail: dhko@yonsei.ac.kr
DOI: 10.1557/jmr.2017.221

https://doi.org/10.1557/jmr.2017.221 Published online by Cambridge University Press

 © Materials Research Society 2017

experiments was limited up to 20 at.%, since the severe volume shrinkage was observed upon crystallization over 20 at.% of the Se concentration. To verify these expected advantages, we investigated the electrical and thermal properties of Se-doped $Ge_{10}Sb_{90}$ thin films.

II. EXPERIMENTAL SECTION

Se-doped $Ge_{10}Sb_{90}$ films with a thickness of 100 nm were deposited onto SiO_2/Si(100) and quartz substrates by a direct current (DC) magnetron co-sputtering method using $Ge_{10}Sb_{90}$ and Pure Se targets in an Ar atmosphere. The base pressure was 5.0×10^{-8} torr, and the working pressure was 1.0×10^{-3} torr. The ratio of $Ge_{10}Sb_{90}$ to Se was varied from 40:1 to 8:1 by separately controlling the sputtering power of the $Ge_{10}Sb_{90}$ and Se targets. The chemical compositions of the deposited films were determined by X-ray photoelectron spectroscopy (XPS; K-alpha, Thermo Scientific Inc., Waltham, Massachusetts). The crystallization temperature and activation energy were analyzed using a differential scanning calorimeter (DSC; DSC 8000, Perkin Elmer, Waltham, Massachusetts). The crystallization temperature was measured at a heating rate of 10 °C/min, and the activation energy was investigated at four heating rates (5, 10, 15, and 20 °C/min). The electrical resistance of the thin films was measured *in situ* as a function of temperature at different heating rates (10–30 °C/min) or isothermal holding temperatures slightly below the crystallization temperature, using a typical two-probe method in a vacuum chamber. To determine the band gap of $Se_x(Ge_{10}Sb_{90})_{100-x}$ films, ultraviolet-visible-near-infrared (UV-Vis-NIR) spectrophotometer (UV-Vis, Cary 5000, Agilent, Santa Clara, California) was used on the films deposited on quartz substrates. To evaluate the electrical properties of the PCM cell, A Keysight B1500A semiconductor device analyzer (Keysight Technologies Inc., Santa Rosa, California) with a pulse-generation system was used. The size of the contact hole was 600 nm, and TiN was used as the top electrode and bottom heater. The phase-change material active layer was 100 nm thick, which was based on the Se-doped $Ge_{10}Sb_{90}$ films, and was deposited between the top electrode and bottom heater. Reversible resistance switching was performed by a SET-RESET pulse and read by a READ pulse.

III. RESULTS AND DISCUSSION

The thermal behaviors of Se-doped $Ge_{10}Sb_{90}$ films were investigated by DSC at various heating rates. To analyze the crystallization temperature and activation energy, powder samples scratched from thin films of Se-doped $Ge_{10}Sb_{90}$ were used. Figure 1 shows the crystallization temperature (T_c) of the Se-doped $Ge_{10}Sb_{90}$ films as a function of Se concentration at a heating rate of 10 °C/min. The crystallization temperature increased

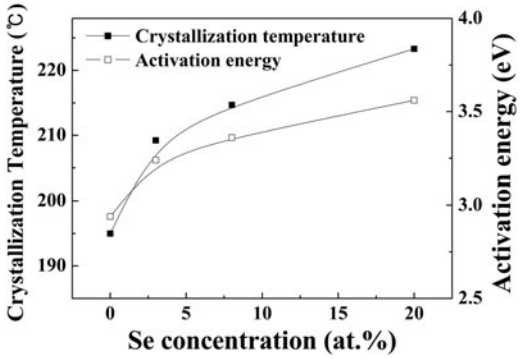


FIG. 1. Crystallization temperature and activation energy as a function of Se concentration in Se-doped $Ge_{10}Sb_{90}$ films.

from 195 to 223 °C as the Se content increased from 0 to 20 at.%. The crystallization temperature is well known to increase with the addition of elements that increase the average bond enthalpy. The type of bonds expected to exist in $Se_x(Ge_{10}Sb_{90})_{100-x}$ films are Ge–Ge (189 kJ/mol), Sb–Sb (126 kJ/mol), Se–Se (206 kJ/mol), Sb–Se (214 kJ/mol), and Ge–Se (235 kJ/mol) bonds.[18] A previous report showed that Se atoms tend to bond with different elements, e.g., Ge or Sb, rather other Se atoms,[19] and heteronuclear bonds have larger bond enthalpy than homonuclear bonds.[20,21] Therefore, the increasing concentration of Se can increase the Ge–Se and Sb–Se bond densities, and these bonds have higher bond energies than Ge–Ge and Sb–Sb bonds and can lead to an increase in the average bond enthalpy. Thus, the increase in the average bond enthalpy may reasonably result in a higher crystallization temperature for the phase transition. The Kissinger equation can be used to evaluate the crystallization activation energy.[22] The linear slope of the Kissinger plot can calculate the crystallization activation energy with four different crystallization temperatures at different heating rates from 5 to 20 °C/min. The crystallization activation energies are shown in Fig. 1. The activation energy for undoped $Ge_{10}Sb_{90}$ and 20 at.% Se-doped films are 2.94 eV and 3.56 eV, respectively, and this energy increased continuously with the increasing Se concentration. In general, the crystallization activation energy is considered proportional to the average bond enthalpy, which agrees well with the results above. Therefore, the addition of Se can rationally be considered to stabilize the amorphous phase, thus enhancing the thermal stability of PRAM devices.

Kinetics analyses of Se-doped $Ge_{10}Sb_{90}$ films were performed by nonisothermal temperature-resistance measurements. The effective overall reaction rate (K) is determined by the following equation, which is a type of Arrhenius equation, $K = K_0 \exp(-E_a/k_bT)$, where K is the effective overall reaction rate, K_0 is the rate factor, E_a is the activation energy, K_b is the Boltzmann constant, and T is the temperature. The rate factor is the

https://doi.org/10.1557/jmr.2017.221 Published online by Cambridge University Press

crystallization kinetic parameter estimated by the Kissinger equation,[22] i.e., $\ln[\alpha/T_c^2] = C + E_a/(k_bT)$, where α is the heating rate. K_0 can be calculated as the exponential of the y-intercept of the fitted line from the Kissinger plot. As shown in Fig. 2, K_0 increased with the increasing concentration of Se. Specifically, the K_0 values of films with Se concentrations of 0, 3, 8, and 20 at.% are 5.25×10^{30}, 1.31×10^{31}, 1.24×10^{32}, and 3.13×10^{33} min^{-1}, respectively. According to previous reports, K_0 is associated with the vibration frequency of an atom, the shape factor during grain growth, and the distance of atomic movement.[23,24] A higher K_0 value may feasibly indicate a high transformation rate. Therefore, PRAM devices made from Se-doped $Ge_{10}Sb_{90}$ films with high Se concentrations may be able to operate at a faster operation speed than the corresponding films with low Se concentrations.

Isothermal crystallization kinetics was used to estimate the thermal stability for PRAM applications. Data retention is one of the important criteria for reliability, and it can be measured by extrapolation from the isothermal Arrhenius plot, which is plotted from the logarithm of the failure time versus $1/k_bT$.[25] The temperatures involved are below the crystallization temperature of Se-doped $Ge_{10}Sb_{90}$ films, and the failure time is defined as the time required for the resistance to decline to 50% of its original value at the given isothermal temperature, as shown in Fig. 3(a). Figure 3(b) shows the extrapolated temperature corresponding to data retention for a period of ten years (i.e., the ten-year archival life temperature, T_{10y}) using films with various Se concentrations. In other words, T_{10y} is the maximum temperature at which data can be retained for ten years, and it increases with the increasing Se concentration. A higher T_{10y} indicates the enhanced stability of the amorphous phase of the phase-change material, and a material with such stability has a higher crystallization temperature and crystallization activation energy than materials with a low T_{10y}. The $Ge_{10}Sb_{90}$, $Se_3(Ge_{10}Sb_{90})_{97}$, $Se_8(Ge_{10}Sb_{90})_{92}$, and $Se_{20}(Ge_{10}Sb_{90})_{80}$ exhibited T_{10y} values of 91, 101, 108, 130 °C, respectively, which are all higher than that of $Ge_2Sb_2Te_5$, namely, 86 °C, as shown in Fig. 3(b). These results indicate that the films with high Se concentrations have better thermal stability than films with low Se concentrations, which is consistent with the results above.

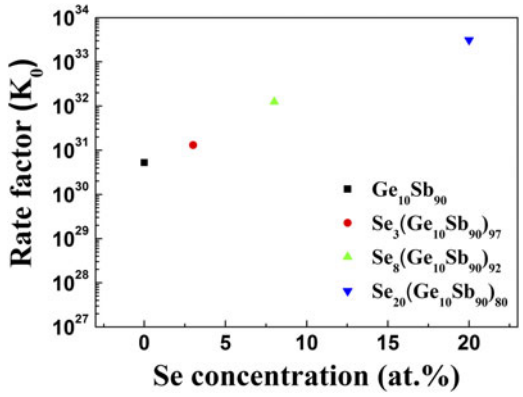


FIG. 2. Rate factor (K_0) of Se-doped $Ge_{10}Sb_{90}$ films as a function of Se concentration.

Figure 4 shows the electrical current–voltage (I–V) properties of the PCM device fabricated from $Se_x(Ge_{10}Sb_{90})_{100-x}$ films with various Se concentrations. The I–V measurements were conducted by applying a DC current sweep. The devices using Se-doped $Ge_{10}Sb_{90}$ films had the same thickness and electrode size. As shown in Fig. 4, the as-deposited films were amorphous in the initial state with high resistance. All the devices switched from the OFF state with high resistance to the ON state with low resistance when the applied voltage exceeded the threshold voltage (V_{th}). The device remained in the low-resistance ON state when the second current sweep was applied. Thus, the I–V curve reveals the typical memory-switching behavior.[26,27] The threshold voltage V_{th} for $Se_x(Ge_{10}Sb_{90})_{100-x}$ films increased from 1.35 to 5.14 V when the Se concentration reached 20 at.%. This may be because Se doping results in increase in the average bond enthalpy and amorphous phase stability. Figure 4 shows the dynamic resistance R_d in the programming region. As the Se concentration increased, the dynamic resistance monotonically increased, thus increasing the resistance of the crystalline

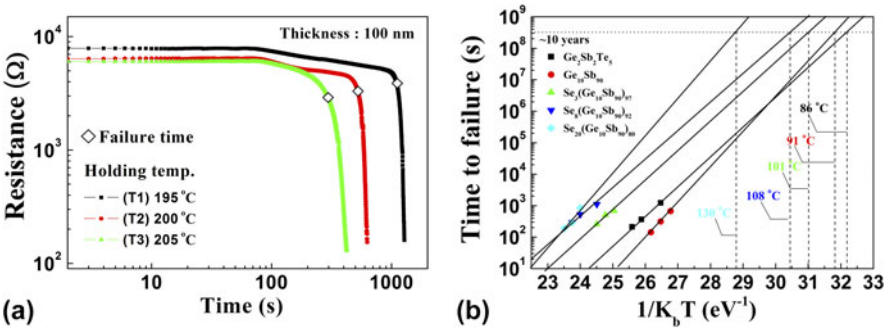


FIG. 3. (a) Electrical resistance of $Se_8(Ge_{10}Sb_{90})_{92}$ film at different isothermal holding temperatures, and (b) Time to failure as a function of reciprocal temperature with various Se concentrations in Se-doped $Ge_{10}Sb_{90}$ films and $Ge_2Sb_2Te_5$.

https://doi.org/10.1557/jmr.2017.221 Published online by Cambridge University Press

state film. The R_d vale of the Se-doped $Ge_{10}Sb_{90}$ films increased from 1535 to 5860 Ω with the increasing Se concentration up to 20 at.%. During the writing operation, the dynamic resistance acts as the load resistance.[28] The highest Se concentration yields the highest load resistance, which may signify that a smaller current is required to generate heat. Thus, the power delivery becomes more effective for the writing operation. Therefore, high Se concentrations in $Se_x(Ge_{10}Sb_{90})_{100-x}$ films should lead to a lower writing current than low Se concentrations.

UV-Vis-NIR spectrophotometer analyses were performed to determine the band gap of the Se-doped $Ge_{10}Sb_{90}$ films. As shown in Fig. 5, the band gap increased from 0.33 eV for the $Ge_{10}Sb_{90}$ film to 0.64 eV for the $Se_{20}(Ge_{10}Sb_{90})_{80}$ film. Thus, Se-doped $Ge_{10}Sb_{90}$ films with high Se concentrations have a larger band gap than films with less Se. In the literature, the band gap of Se is larger than that of Ge or Sb.[29,30] The observed increase in the band gap is related to the higher resistance and lower electrical conductivity of the film.[31] Generally, electrons cannot move as easily from the valence band to the conduction band when the band gap is larger. Therefore, the increase in band gap with the Se concentration is expected to reduce the operation current and increase the crystallization activation energy, which improves the amorphous phase stability.

To investigate the resistance–current (*R–I*) curves of the PCM device employing $Se_x(Ge_{10}Sb_{90})_{100-x}$ films, a RESET pulse was applied to the devices, which was analyzed using a read voltage pulse of 0.2 V. The applied pulse width was 100 ns. Figure 6 shows the resistance as a function of the programming current for several Se concentrations. The resistance of the devices with higher Se contents increased more abruptly with the increasing programming current than that of the devices with less Se. Moreover, both the set (i.e., the crystalline state) and reset (i.e., the amorphous state) resistances of the device increased with the increasing Se concentration. The electrical characteristics of PRAM devices with various Se-doped and undoped $Ge_{10}Sb_{90}$ films are summarized in Table I. In addition, the set and reset resistances are shown in Table I.

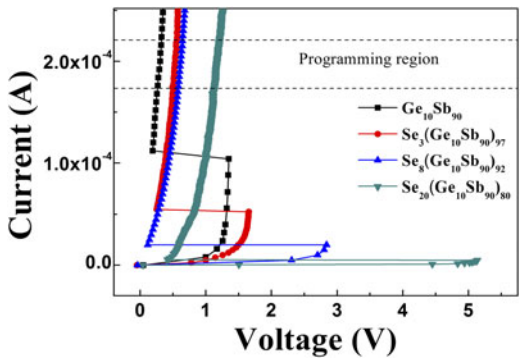


FIG. 4. Current versus voltage curves for Se-doped $Ge_{10}Sb_{90}$ films with various Se concentrations.

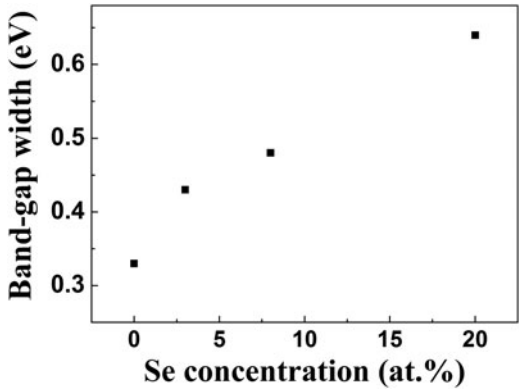


FIG. 5. Band gap of Se-doped $Ge_{10}Sb_{90}$ films as a function of Se concentration.

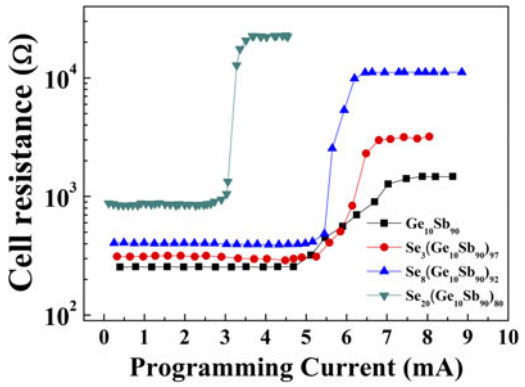


FIG. 6. Cell resistance as a function of programming current (i.e., *R–I* curves) for Se-doped $Ge_{10}Sb_{90}$ film device with various Se concentrations.

TABLE I. RESET current, RESET resistance, SET resistance, SET operation time, programming window, and maximum ten-year data retention temperature of undoped and Se-doped $Ge_{10}Sb_{90}$ films.

	$Ge_{10}Sb_{90}$	$Se_3(Ge_{10}Sb_{90})_{97}$	$Se_8(Ge_{10}Sb_{90})_{92}$	$Se_{20}(Ge_{10}Sb_{90})_{80}$
RESET current (mA)	7.87	6.82	6.47	3.64
RESET resistance (kΩ)	1.49	3.18	11.15	22.60
SET resistance (kΩ)	0.23	0.3	0.4	0.85
SET operation time (ns)	100	90	60	30
Programming window	6	10	29	26
Data retention temperature of 10 years (T_{10y})	91	101	108	130

https://doi.org/10.1557/jmr.2017.221 Published online by Cambridge University Press

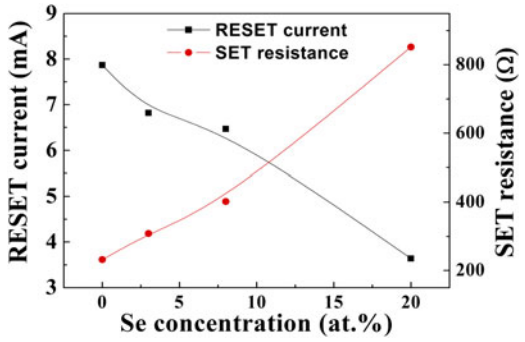


FIG. 7. Reset current and set resistance variations as a function of Se concentration in Se-doped $Ge_{10}Sb_{90}$ film devices.

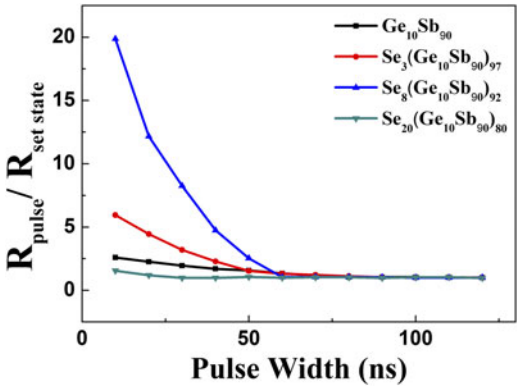


FIG. 8. Ratio of the resistances reached after applying a pulse to an amorphous cell and the resistance of the SET state, which is plotted versus the width of applied pulse for several Se concentrations.

We also analyzed the effect of Se on the reset current and set resistance of Se-doped $Ge_{10}Sb_{90}$ films. Figure 7 shows the reset current and set resistance as a function of Se concentration. With the increase in the Se concentration from 0 to 20 at.%, the reset current decreases from 7.87 to 3.64 mA (see also Table I), and the set resistance increases from 232 to 852 Ω. These results demonstrate that the reset current is closely related to the set resistance of the Se-doped $Ge_{10}Sb_{90}$ films because the efficacy of joule heating, which is based on a power law, increases with the increasing resistance of phase-change material. These results indicate that the operation properties of Se-doped $Ge_{10}Sb_{90}$ films can be enhanced by higher set and reset resistances, which are advantageous for reducing the operation current of memory devices. This is consistent with our above-mentioned results.

The operation time of PRAM devices is comprised of set and reset operation times. The reset operation time (i.e., the amorphization time) is shorter than the set operation time (i.e., the crystallization time) because full crystallization requires a longer time than amorphization (i.e., the quenching time). Therefore, the set operation time dominates the operation time for the PRAM devices in general. To compare the crystallization speed (i.e., the crystallization time) of the Se-doped $Ge_{10}Sb_{90}$ films, the $R_{pulse}/R_{set\ state}$ ratio was measured in the PRAM devices. R_{pulse} is the resistance of the cell under the applied voltage, and $R_{set\ state}$ is the lowest cell resistance of Se-doped $Ge_{10}Sb_{90}$ films. When the $R_{pulse}/R_{set\ state}$ ratio is close to one, the cell is in the set state. Figure 8 shows the $R_{pulse}/R_{set\ state}$ ratio as a function of the applied pulse width for various Se concentrations. This curve reflects the crystallization speed, and the amplitude of the applied pulse is determined by the voltage that results in the lowest cell resistance for a cell in the reset state. As shown in Fig. 8, the Se-doped $Ge_{10}Sb_{90}$ films with low Se concentration devices are obviously less crystallized after short pulses than the films with high Se concentration devices. Table I shows the set operation times for all the $Ge_{10}Sb_{90}$-based devices, which is calculated by the time required to achieve a $R_{pulse}/R_{set\ state}$ ratio of 0.99. This result means that the PRAM device made from a film with a high Se concentration would have improved operation speed (i.e., a short crystallization time).

Table I shows the programming window of all the Se-doped $Ge_{10}Sb_{90}$ films. The programming window is calculated based on the difference between R_{set} and R_{reset} (measured from Fig. 6), and it increases with the increasing Se concentration from 6 for the undoped $Ge_{10}Sb_{90}$ film to 26 for $Se_{20}(Ge_{10}Sb_{90})_{80}$ film. A larger programming window enables a large signal margin, which can provide a desirable signal-to-noise ratio.[17] Therefore, we expect that the Se-doped $Ge_{10}Sb_{90}$ films with a high Se concentration will provide better reliability than the films with a low Se concentration.

IV. CONCLUSION

In this study, we evaluated the thermal and electrical characteristics of $Se_x(Ge_{10}Sb_{90})_{100-x}$ films as a phase-change material by doping elemental Se into $Ge_{10}Sb_{90}$ films. The crystallization temperature was measured up to 223 °C, and the films with high Se concentrations showed good thermal stability due to the increase in the Se concentration. In addition, the crystallization activation energy and data retention temperature were increased with the increasing Se concentration. The rate factor for undoped $Ge_{10}Sb_{90}$ and 20 at.% Se-doped films were 5.25 $\times$ 10^{30} and 3.13 $\times$ 10^{33} min^{-1}, respectively. Measurements performed using a UV-Vis-NIR spectrophotometer confirmed that the band gap increases from 0.33 eV for the $Ge_{10}Sb_{90}$ film to 0.64 eV for the $Se_{20}(Ge_{10}Sb_{90})_{80}$ film. It should be noted that the measured activation energy, data retention, rate factor, and band-gap width values are experimental results of the as-deposited materials, not of the melt-quenched materials in the actual devices, which might produce differences in the experimental results.[32,33] Therefore, these results should be verified in melt-quenched materials for the application to the actual devices.

https://doi.org/10.1557/jmr.2017.221 Published online by Cambridge University Press

The electrical performance of Se-doped $Ge_{10}Sb_{90}$ films was superior to that of the undoped $Ge_{10}Sb_{90}$ film. The resistance of both the set and reset states of the device increases with the Se concentration. At high Se concentrations, the Se-doped $Ge_{10}Sb_{90}$ film demonstrated a high threshold voltage and high load resistance. The reset current decreased with the increasing Se concentration. In addition, a faster transition between the amorphous and the crystalline states was observed in the films with higher Se concentration. Finally, the programming window for Se-doped $Ge_{10}Sb_{90}$ films increased from 6 to 26 from 0 to 20 at.% Se. In summary, the $Se_{20}(Ge_{10}Sb_{90})_{80}$ film, which had the highest Se concentration (i.e., 20 at.%), exhibited the highest thermal stability, threshold voltage, largest band gap, ten-year data retention temperature, the highest speed, the lowest power consumption, and the highest reliability of all the films investigated. This could translate into reduced writing currents, improved amorphous phase stability, faster operation speeds, and better reliability. Therefore, Se-doped $Ge_{10}Sb_{90}$ films are a significantly promising candidate for high-performance PRAM devices.

ACKNOWLEDGMENTS

This study was supported by grants from the R&D Program for Industrial Core Technology funded by the Ministry of Trade, Industry, and Energy (MOTIE), Republic of Korea (Grant No. 10039200) and the Joint Program for Samsung Electronics–Yonsei University by Samsung Research Funding Center for Future Technology (SRFC-MA1502-01).

REFERENCES

1. M.H. Kryder and C.S. Kim: After hard drives-what comes next? *IEEE Trans. Magn.* **45**, 3406 (2009).
2. R.E. Simpson, M. Krbal, P. Fons, A.V. Kolobov, J. Tominaga, T. Uruga, and H. Tanida: Toward the ultimate limit of phase change in $Ge_2Sb_2Te_5$. *Nano Lett.* **10**, 414 (2010).
3. S.J. Ahn, Y.N. Hwang, Y.J. Song, S.H. Lee, S.Y. Lee, J.H. Park, C.W. Jeong, K.C. Ryoo, J.M. Shin, J.H. Park, Y. Fai, J.H. Oh, G.H. Koh, G.T. Jeong, S.H. Joo, S.H. Choi, Y.H. Son, J.C. Shin, Y.T. Kim, H.S. Jeong, and K. Kim: Highly reliable 50 nm contact cell technology for 256 Mb PRAM. In *Symposium on VLSI Technology Digest of Technical Papers* (IEEE Symposium on VLSI Technology, Kyoto, Japan, 2005); pp. 98–99.
4. S.L. Cho, J.H. Yi, Y.H. Ha, B.J. Kuh, C.M. Lee, J.H. Park, S.D. Nam, H. Horii, B.O. Cho, K.C. Ryoo, S.O. Park, H.S. Kim, U.I. Chung, J.T. Moon, and B.I. Ryu: Highly scalable on-axis confined cell structure for high density PRAM beyond 256 Mb. In *Symposium on VLSI Technology Digest of Technical Papers* (IEEE Symposium on VLSI Technology, Kyoto, Japan, 2005); pp. 96–97.
5. F. Xiong, M.H. Bae, Y. Dai, A.D. Liao, A. Behnam, E.A. Carrion, S. Hong, D. Ielmini, and E. Pop: Self-aligned nanotube-nanowire phase change memory. *Nano Lett.* **13**, 464 (2013).
6. S-W. Nam, H-S. Chung, Y.C. Lo, L. Qi, J. Li, Y. Lu, A.T.C. Johnson, Y.W. Jung, P. Nukala, and R. Agarwal: Electrical wind force-driven and dislocation-templated amorphization in phase-change nanowires. *Science* **336**, 1561 (2012).
7. M. Terao, T. Morikawa, and T. Ohta: Electrical phase-change memory: Fundamentals and state of the art. *Jpn. J. Appl. Phys.* **48**, 080001 (2009).
8. D. Loke, T.H. Lee, W.J. Wang, L.P. Shi, R. Zhao, Y.C. Yeo, T.C. Chong, and S.R. Elliott: Breaking the speed limits of phase-change memory. *Science* **336**, 1566 (2012).
9. S. Lai and T. Lowrey: OUM-A 180 nm nonvolatile memory cell element technology for stand alone and embedded applications. In *IEEE IEDM Tech. Dig.* (IEEE International Electron Devices Meeting, Washington, DC, 2001); pp. 36.5.1–36.5.4.
10. N. Takaura, T. Ohyanagi, M. Tai, M. Kitamura, M. Kinoshita, K. Akita, T. Morikawa, S. Kato, M. Araidai, K. Kamiya, T. Yamamoto, and K. Shiraishi: Understanding the switching mechanism of charge-injection $GeTe/Sb_2Te_3$ phase change memory through electrical measurement and analysis of 1R test structure. In *ICMTS* (IEEE International Conference, Udine, Italy, 2014); pp. 32–37.
11. S. Hosaka, K.M. Tamura, H. Sone, and H. Koyanagi: Proposal for a memory transistor using phase-change and nanosize effects. *Microelectron. Eng.* **73–74**, 736 (2004).
12. J.D. Maimon, K.K. Hunt, L. Burcin, and J. Rodgers: Chalcogenide memory arrays: Characterization and radiation effects. *IEEE Trans. Nucl. Sci.* **50**, 1878 (2003).
13. L. Van Pieterson, M.H.R. Lankhrst, M. Van Schijndel, A.E.T. Kuiper, and J.H.J. Roosen: Phase change recording materials with a growth-dominated crystallization mechanism: A materials overview. *J. Appl. Phys.* **97**, 083520 (2005).
14. H.Y. Cheng, T.H. Hsu, S. Raoux, J.Y. Wu, P.Y. Du, M. Breitwisch, Y. Zhu, E.K. Lai, E. Joseph, S. Mittal, R. Cheek, A. Schrott, S.C. Lai, H.L. Lung, and C. Lam: A high performance phase change memory with fast switching speed and high temperature retention by engineering the $Ge_xSb_yTe_z$ phase change material. Presented at the *Electron Devices Meeting, IEDM 2011* (IEEE International, Washington, DC, 2011); pp. 3.4.1–3.4.4.
15. S. Rauox, H-Y. Cheng, J. Sandrini, J. Li, and J. Jordan-Sweet: Materials engineering for phase change random access memory. In *Non-Volatile Memory Technology Symposium (NVMTS), 2011 11th Annual* (IEEE, Shanghai, China, 2011); pp. 1–5.
16. M.J. Kang, T.J. Park, D. Wamwangi, K. Wang, C. Steimer, S.Y. Choi, and M. Wuttig: Electrical properties and crystallization behavior of Sb_xSe_{100-x} thin films. *Microsyst. Technol.* **13**, 153 (2007).
17. M.J. Kang, S.Y. Choi, D. Wamwangi, K. Wang, C. Steimer, and M. Wuttig: Structural transformation of Sb_xSe_{100-x} thin films for phase change nonvolatile memory applications. *J. Appl. Phys.* **98**, 014904 (2005).
18. A. Giridhar, P.S.L. Narasimham, and S. Mahadevan: Electrical properties of GeSbSe glasses. *J. Non-Cryst. Solids* **37**, 165 (1980).
19. S.A. Saleh: Synthesis and characterization of $Sb_{65}Se_{35-x}Ge_x$ alloys. *Mater. Sci. Appl.* **2**, 950 (2011).
20. W.H. Zachariasen: The atomic arrangement in glass. *J. Am. Chem. Soc.* **54**, 3841 (1932).
21. L. Pauling: *The Nature of the Chemical Bond and the Structure of Molecules and Crystals: An Introduction to Modern Structural Chemistry*, 3rd ed. (Cornell University, New York, 1960); ch. 3.
22. H.E. Kissinger: Reaction kinetics in differential thermal analysis. *Anal. Chem.* **29**, 1702 (1957).
23. P.C. Chang, C.C. Chang, S.C. Chang, and T.S. Chin: Crystallization behavior of Si-added amorphous $Ga_{19}Sb_{81}$ films for phase-change memory. *J. Non-Cryst. Solids* **383**, 106 (2014).
24. H.Y. Cheng, K.F. Kao, C.M. Lee, and T.S. Chin: Crystallization kinetics of Ga–Sb–Te films for phase change memory. *Thin Solid Films* **516**, 5513 (2008).
25. W.A. Johnson and R.F. Mehl: Reaction kinetics in processes of nucleation and growth. *Trans. Am. Inst. Min., Metall. Pet. Eng.* **135**, 416 (1939).

https://doi.org/10.1557/jmr.2017.221 Published online by Cambridge University Press

26. H. Lee, Y.K. Kim, D. Kim, and D.H. Kang: Switching behavior of indium selenide based phase-change memory cell. *IEEE Trans. Magn.* **41**, 1034 (2005).
27. J. Feng, Y. Zhang, B. Cai, and B. Chen: Thermal stability and electronic structures of N-doped SiSb films for high temperature applications of phase-change memory. *Appl. Phys. A* **97**, 507 (2009).
28. Y.N. Hwang, S.H. Lee, S.J. Ahn, S.Y. Lee, K.C. Ryoo, H.S. Hong, H.C. Koo, F. Yeung, J.H. Oh, H.J. Kim, W.C. Jeong, J.H. Park, H. Horii, Y.H. Ha, J.H. Yi, G.H. Koh, G.T. Jeong, H.S. Jeong, and K.N. Kim: Writing current reduction for high-density phase-change RAM. In *IEEE IEDM Tech. Dig.* (IEEE International Electron Devices Meeting, Washington, DC, 2003); pp. 37.1.1–37.1.4.
29. O. Madelung, U. Rössler, and M. Schulz: *Non-Tetrahedrally Bonded Elements and Binary Compounds I*, 1st ed. (Springer, Heidelberg, 1998).
30. A.K. Bhatnagar, K.V. Reddy, and V. Srivastava: Optical energy gap of amorphous selenium: Effect of annealing. *J. Phys. D: Appl. Phys.* **18**, L149 (1985).
31. X. Zhou, L. Wu, Z. Song, F. Rao, M. Zhu, C. Peng, D. Yao, S. Song, B. Liu, and S. Feng: Carbon-doped $Ge_2Sb_2Te_5$ phase change material: A candidate for high-density phase change memory application. *Appl. Phys. Lett.* **101**, 142104 (2012).
32. K.H. Do, D.K. Lee, H.C. Sohn, M-H. Cho, and D-H. Ko: Crystallization behaviors of laser induced $Ge_2Sb_2Te_5$ in different amorphous states. *J. Electrochem. Soc.* **157**, H264 (2010).
33. K.H. Do, D.K. Lee, J-H. Bae, D-H. Ko, H.C. Sohn, and M-H. Cho: Comparison of the crystallization behaviors in as-deposited and melt-quenched N-doped $Ge_2Sb_2Te_5$ Thin films. *J. Electrochem. Soc.* **158**, H347 (2011).

Supplementary Material

To view supplementary material for this article, please visit https://doi.org/10.1557/jmr.2017.221.

https://doi.org/10.1557/jmr.2017.221 Published online by Cambridge University Press